532.527

Paper No. 191-6

A Study on the Vortex Oscillator (2nd Report: Oscillatory Phenomena Occurring in a Confined Vortex Oscillator)*

By Shoji TAKAGI**, Yuji YOKOYA***

A vortex oscillator, which has a double input vortex chamber and two conduit-capacity systems, is studied theoretically and experimentally. An oscillator with a single conduit-capacity system is also examined. A mathematical model of this type of oscillator is presented and its validity is examined by experiments. The stability of the equilibrium state of the system is discussed. Higher modes of oscillation occur in the system under certain conditions when the compressibility of the working fluid is relatively large. The frequency of the higher mode coincides with the natural frequency of the same mode of the conduit-capacity system of the oscillator. Relaxation oscillations occur under certain conditions also. The experimental data were found to be in good agreement with theoretical predictions.

1. Introduction

In a previous paper[2], we have proposed a mathematical model of a fluidic oscillator which consists of a vortex valve with double inputs and two conduit-capacity systems (i. e. a confined vortex oscillator[1]), on the assumption that the compressibility of the working fluid could be ignored. The validity of the model has been examined by experiments.

On the other hand, oscillatory phenomena which can not be predicted by the above mentioned model may occur in systems with gases as the working fluids. These oscillations are studied in this paper. First we discuss a mathematical model of a system in which the compressibility of the fluid is taken into account. Next we make analyses using the mathematical model and examine the validity of the model by experiments.

2. Mathematical model of oscillator

2.1 Steady state characteristics of vortex valve

Figure 1 shows a test vortex valve. The fluid enters the vortex chamber through two input ports A, B and flows out of the orifice D into the atmosphere. Experimental results of steady state characteristics of this valve are shown in Fig.2. The pressures at the periphery of the vortex chamber P_{Os} (which were measured at C in Fig.1) are plotted against the flow rate Q_{1s} at one of the two input ports of the valve for several values of the flow rate Q_{2s} at the other port. It is seen that P_{Os} depends on Q_{1s} and Q_{2s}. Namely, the steady state characteristics of the valve may be represented by

$$P_{0s}=f(Q_{1s}, Q_{2s}) \quad \cdots\cdots (1)$$

It has been discussed in detail in the previous paper[2] that this representation matches well with a mathematical model for an oscillator with a vortex valve shown in Fig.1. The method of the measurement is the same as the one explained in the previous paper. Air was used as the working fluid.

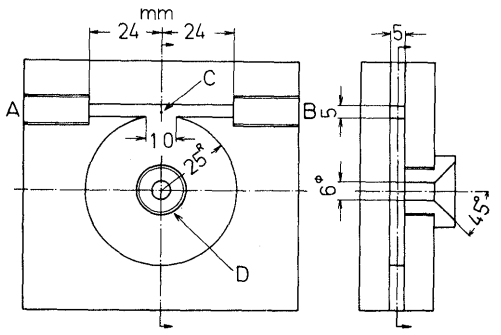

Fig.1 Shape and dimensions of test vortex valve

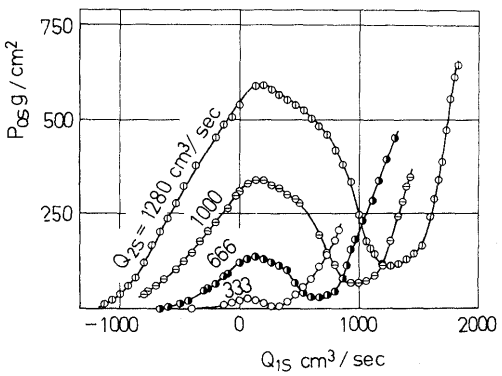

Fig.2 Steady state characteristics of the vortex valve

* Received 4th October, 1978.
** Associate Professor, School of Energy Engineering, Toyohashi Univ. of Technology, Toyohashi 440, Japan.
*** Engineer, Toyota Motor Co., Ltd.

Though the function f in the right hand side of Eq.(1) can be discussed qualitatively in a theoretical manner, it is determined by the use of the experimental results here. Let us now assume the relation between flow rate Q_s out of the outlet orifice and P_{os} in the form of

$$Q_s=Q_{1s}+Q_{2s}=CA_0\sqrt{2P_{0s}/\rho} \quad \cdots\cdots(2)$$

where C is the dischage coefficient, A_O is the opening area of the orifice, and ρ is the density of air. The dischage coefficient C is plotted against Q_{1s}/Q_{2s} in Fig.3 for four different values of Q_{2s}. This figure shows that the coefficient C may be determined as a function of Q_{1s}/Q_{2s}. Thus Eq.(2) reduces to

$$P_{0s}=F(Q_{is}/Q_{js})(Q_{1s}+Q_{2s})^2 \qquad (i,j=1,2\ ;\ i\neq j) \quad \cdots\cdots(3)$$

where $F(Q_{is}/Q_{js})$ $[=\rho/2A_O^2C^2]$ means a function of Q_{is}/Q_{js}, and is symmetric with respect to the plane $Q_{1s}=Q_{2s}$.

2.2 Fundamental equations

A schematic diagram of the vortex oscillator investigated in this paper is shown in Fig.4, in which Q_{iO} is the constant flow rate into the capacity (i=1,2), P_{vi} is the pressure in the capacity, V_i is the volume of the capacity, Q_{vi} is the flow rate at the capacity end, P_i is the pressure at the valve end, κ_i is the bulk modulus of air in the capacity, Q_i is the flow rate at the valve end, β is the reciprocal of resistance factor in the inlet passage [see Eq.(7)], P_O is the pressure at the periphery of the vortex chamber, A is the cross sectional area of the conduit, l_i is the length of the conduit, and the subscripts 1 and 2 correspond to the left side conduit-capacity system and the right side one

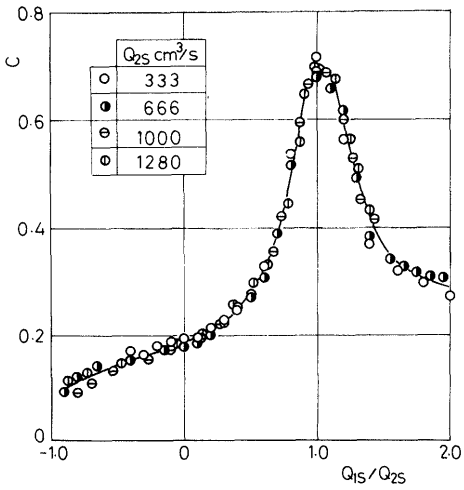

Fig.3 Discharge coefficient of the valve outlet orifice

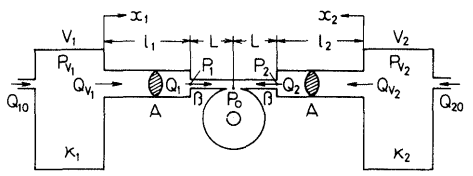

Fig.4 Schematic diagram of the confined vortex oscillator

respectively.

We derive fundamental equations of the system on the basis of the following assumptions: (i) Q_{iO} is kept constant. (ii) The characteristics of the vortex valve in operation are the same as the steady state ones. (iii) Motion of the fluid in the conduits follows the one-dimensional wave equation without friction.

The pressure $\hat{P}_i$ and the flow rate $\hat{Q}_i$ at a certain position in the conduit may be given by

$$\hat{P}_i=\hat{P}_{i0}+Z_c\{\psi_{1i}(t-x_i/c)+\psi_{2i}(t+x_i/c)\} \quad \cdots\cdots(4\cdot a)$$

$$\hat{Q}_i=\hat{Q}_{i0}+\psi_{1i}(t-x_i/c)-\psi_{2i}(t+x_i/c) \quad \cdots\cdots(4\cdot b)$$

where $\hat{P}_{iO}$ and $\hat{Q}_{iO}$ are constants, ψ_{1i} and ψ_{2i} are wave functions, $Z_C=\rho c/A$, c is the velocity of wave propagation, and t is the time. Boundary conditions at both ends of conduits are

$$\hat{P}_i=P_{Vi},\ \hat{Q}_i=Q_{Vi} \qquad \text{at} \quad x_i=0 \quad \cdots\cdots(5\cdot a)$$

$$\hat{P}_i=P_i,\ \hat{Q}_i=Q_i \qquad \text{at} \quad x_i=l_i \quad \cdots\cdots(5\cdot b)$$

The pressure change in the capacity is expressed as

$$\dot{P}_{Vi}=(\kappa_i/V_i)(Q_{i0}-Q_{Vi}) \quad \cdots\cdots(6)$$

where a dot $\dot{}$ indicates differentiation with respect to t. Let us express the relation between Q_i and (P_i-P_O) as follows:

$$Q_i=\beta(P_i-P_0) \quad \cdots\cdots(7)$$

The characteristics of the vortex valve is written as

$$P_0=f(Q_1,Q_2) \quad \cdots\cdots(8)$$

Equation (8) represents the characteristic curved surface of the vortex valve in the three-dimensional coordinate system (Q_1,Q_2,P_O), and it has the following properties[2].

$$\left.\begin{array}{lll} E_1>0 & \text{when} & Q_1>Q_2 \\ E_2>0 & \text{when} & Q_1<Q_2 \end{array}\right\} \quad \cdots\cdots(9)$$

where $E_1=(\partial f/\partial Q_1)$ and $E_2=(\partial f/\partial Q_2)$ (see Fig.2).

Equations (4)∿(8) are the fundamental equations describing the operation of the oscillator.

3. Analyses of the mathematical model

3.1 Stability of the system

The equilibrium state of the system is obtained by setting terms differentiated with respect to t and the wave functions in the fundamental equations equal to zero. Then the flow rates are given by $Q_i=Q_{vi}=Q_{iO}$ (i=1, 2). Linearizing the fundamental equations about the equilibrium state, and assuming that the deviations of all quantities from the equilibrium state are proportional to e^{st}, we obtain the eigen value equation as

$$\begin{aligned}&\{(Z_c+D_1)(Z_c+D_2)-E_1E_2\}(1+C_1s)(1\\&+C_2s)e^{(\tau_1+\tau_2)s}+\{(Z_c-D_1)(Z_c-D_2)\\&-E_1E_2\}(1-C_1s)(1-C_2s)e^{-(\tau_1+\tau_2)s}\\&+\{(Z_c+D_1)(Z_c-D_2)+E_1E_2\}(1+C_1s)(1\\&-c_2s)e^{(\tau_1-\tau_2)s}+\{(Z_c-D_1)(Z_c+D_2)\\&+E_1E_2\}(1-C_1s)(1+C_2s)e^{(\tau_2-\tau_1)s}=0 \quad \cdots(10)\end{aligned}$$

where $C_i=Z_cV_i/\kappa_i$, $E_i=(\partial f/\partial Q_i)_{Q_1=Q_{10},Q_2=Q_{20}}$, $D_i=E_i+1/\beta$, $\tau_i=l_i/c$, and i=1,2.

It is difficult to discuss generally the stability of the system from Eq.(10). Here the stability is discussed for the cases in which the oscillator has a special configuration or operational conditions.

First the stability is investigated when $Q_{10}=Q_{20}$. A relation $E_1=E_2>0$ holds in this case from the previous discussion[2]. This relation leads to the conclusion that all eigen values of Eq.(10) exist in the left half of the s-plane; that is, when $Q_{10}=Q_{20}$, the oscillator can not operate no matter what geometrical construction it may have.

Next the stability is discussed for the system in which one of the two conduits is sufficiently short by comparison with the other one, i.e. $l_1 \gg l_2$. Then expanding $e^{\pm\tau_2 s}$ in the form of Taylor series and taking only the first two terms of the series (i.e. $e^{\pm\tau_2 s}=1\pm\tau_2 s$), we can derive the following equations from Eq.(10),

$$1+G(s)e^{-2\tau_1 s}=0 \quad \cdots\cdots(11\cdot a)$$

$$G(s)=\frac{(1-C_1 s)(F_1 s^2+F_2 s+F_3)}{(1+C_1 s)(G_1 s^2+G_2 s+G_3)} \quad \cdots\cdots(11\cdot b)$$

where,

$$F_1=Z_c C_2 \tau_2 (Z_c-D_1),$$
$$F_2=(C_2+\tau_2)\{Z_c D_2-(D_1 D_2-E_1 E_2)\},$$
$$F_3=Z_c(Z_c-D_1), \quad G_1=Z_c C_2 \tau_2 (Z_c+D_1),$$
$$G_2=(C_2+\tau_2)\{Z_c D_2+(D_1 D_2-E_1 E_2)\},$$
$$G_3=Z_c(Z_c+D_1)$$

Equation (11.a) can also be derived from the fundamental equations by neglecting the compressibility of the fluid in the shorter conduit. If all roots of Eq.(11.a) locate in the left half of the s-plane, the system is stable. We neglect the resistant factor in the inlet passage of the valve for the sake of the convenience of analyses. Then the quantity $1/\beta$ is equal to zero. The stability of the system is examined by Nyquist criterion[3]. Putting $s=j\omega'$, where $j=\sqrt{-1}$, in Eq.(11.a), and paying attention to the point where a vector $G(j\omega')e^{-2j\omega'\tau_1}$ is led by rotating the vector $G(j\omega')$ by the angle $2\omega'\tau_1$ in the clockwise direction, we can derive some properties of the system necessary to evaluate the stability as follows:

(A) The starting and terminating points of a vector locus $G(j\omega')$ are $G(0)=(Z_c-E_1)/(Z_c+E_1)$ and $G(\infty)=-(Z_c-E_1)/(Z_c+E_1)$, respectively. And their positions relative to the unit circle are determined easily; that is, (i) when $E_1>0$, both $G(0)$ and $G(\infty)$ exist in the unit circle, and (ii) when $E_1<0$, both $G(0)$ and $G(\infty)$ exist outside the unit circle (see Fig.5).

(B) The location of the vector locus relative to the unit circle can be obtained by examining $|G(j\omega')|$. That is,

(i) $G(j\omega')$ exists in the unit circle when $E_1>0$.

(ii) $G(j\omega')$ exists outside the unit circle when $E_1<0$.

In both cases $G(j\omega')$ is tangent to the unit circle at $\omega'=\sqrt{1/C_2\tau_2}$.

(C) It is easily seen from Eq.(11.b) that $G(s)e^{-2\tau_1 s}$ has two poles in the right half s-plane if

$$(Z_c+E_1)E_2<0 \quad \cdots\cdots(12)$$

Under other conditions, Eq.(11.b) has no pole in the right half s-plane. From Eq.(9), E_1 and E_2 are not negative simultaneously. Hence, Eq.(12) is rewritten as follows:

$$E_1>0,\ E_2<0 \quad \text{or} \quad Z_c+E_1<0 \quad \cdots\cdots(13)$$

(D) The vector locus $G(j\omega')$ can be drawn qualitatively as in Fig.5.

The results obtained in (A)∿(D) lead to the conclusions concerning the stability of the system in which $l_1 \gg l_2$. They are summarized as follows: (I) When both E_1 and E_2 are positive, the system is stable, namely the system does not operate. (II) When E_1 is negative, namely when $Q_{10}<Q_{20}$ [see Eq.(9)], the eigen value equation (11.a) has one statically unstable root or more and an infinite number of dynamically unstable roots. This means that a small deviation from the equilibrium state induces a diverging oscillation in an infinite number of modes. (III) When E_2 is negative, namely when $Q_{10}>Q_{20}$, the system has two unstable roots. Considering that the characteristic roots always take the form of complex conjugate in the s-plane, we can conclude that in this case the system oscillates with only one frequency or the equilibrium state falls into instability in a nonoscillatory fashion.

3.2 Stability of oscillator with a single capacity

This section is concerned with an oscillator with a single conduit-capacity system, for instance, an oscillator in which the constant rate of flow Q_{20} is delivered directly to the right side inlet of the valve in Fig.4. Hereafter, we call this type of oscillator a single-capacity-oscillator, and the oscillator treated in the previous section a double-capacity-oscillator.

Here we put $E_2=D_2=\tau_2=0$ in Eq.(11), then the eigen value equation becomes

$$1+\frac{(Z_c-D_1)(1-C_1 s)}{(Z_c+D_1)(1+C_1 s)}e^{-2\tau_1 s}=0 \quad \cdots\cdots(14)$$

The stability can be also discussed by the use of Nyquist criterion. The results obtained are summarized as follows: (I') When $D_1>0$, the system is stable. (II') When $D_1<0$, the system has one statically unstable root and an infinite number of dynamically unstable roots (here, friction loss in the

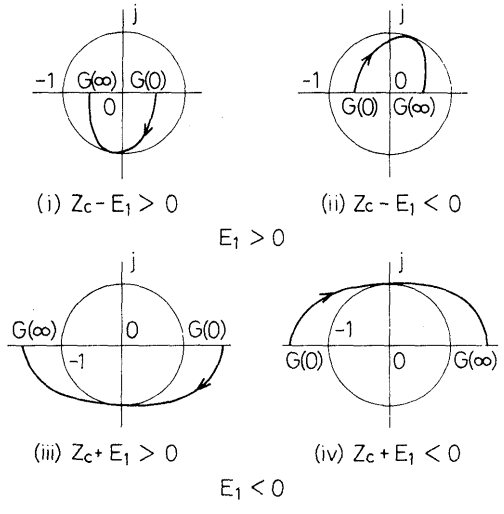

Fig.5 Vector loci of $G(j\omega')$

conduits is ignored). This type of oscillator can operate only if $D_1<0$.

4. Experiments and discussion

4.1 Experimental apparatus and method of experiment

The arrangement of an experimental setup is schematically shown in Fig.6. The constant flow rates Q_{10} and Q_{20} delivered to the capacity were regulated with the valves V_1 and V_2 and were measured by rotameters F_1 and F_2. Pressure drops across the orifices O_1 and O_2 were set so large that both Q_{10} and Q_{20} were kept nearly constant. Oscillations were measured by pressure transducers at several points in the conduits. The diameters of the conduits d_f were 6 and 10 mm, and the length l_i was varied from 0.5 to 30 m.

4.2 Experimental results and discussion

Experimental results concerning both the double- and single-capacity-oscillators are presented here. First the results of the experiment with the double-capacity-oscillator are described.

The analytical conclusion described in section 3.1; that is, the oscillator can not operate if $Q_{10}=Q_{20}$, has been verified by the experiment. Figure 7 shows three examples of measured wave forms. In this figure p_{v1}, p_{v2} and p_1 are pressure fluctuations at the both capacities and at the valve side end of the conduit 1 (i.e. the left side one in Fig.6). The measured frequency f is plotted against the conduit length l_1 in Fig.8. The dot-dash-lines show the calculated frequencies which are frequencies of the small diverging oscillations about the equilibrium state obtained from Eq.(11.a). The solid lines show the numerical solutions for the fundamental equations where a lumped parameter system is used instead of Eqs.(4.a)(4.b) to describe the motion of fluid in the conduits. Lumping of the equation of motion of fluid in the conduits was made in the following way. The longer conduit was divided into four equal-length sections. The fluid in each section was assumed to move as a solid body, and the equivalent capacity equal to the volume of the section was connected to the end of each section. The shorter conduit was regarded as one section. Friction force

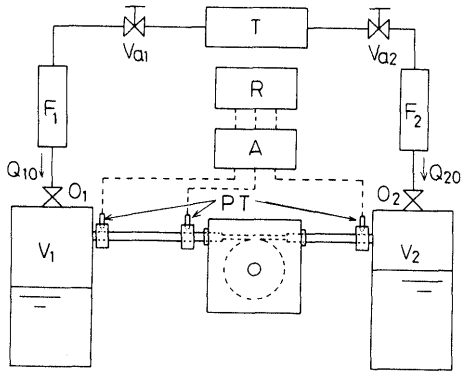

T:tank, V_{ai}:valve, F_i:rotameter, O_i:orifice, PT:pressure transducer, A:amplifier, R:oscillograph

Fig.6 Schematic diagram of the experimental apparatus

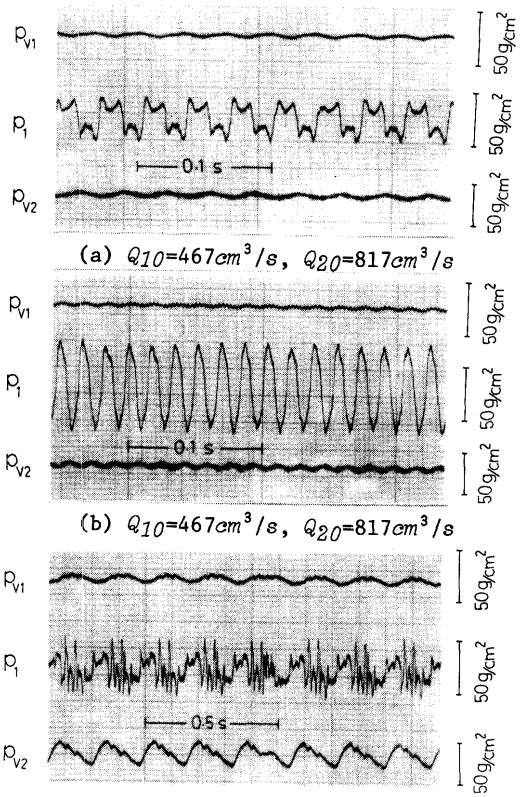

(a) $Q_{10}=467cm^3/s$, $Q_{20}=817cm^3/s$

(b) $Q_{10}=467cm^3/s$, $Q_{20}=817cm^3/s$

(c) $Q_{10}=817cm^3/s$, $Q_{20}=467cm^3/s$

(d_f=10mm, l_1=5m, l_2=0.5m, V_1=3.9l, V_2=2l)

Fig.7 Examples of the wave forms for the double-capacity-oscillator obtained from the experiments

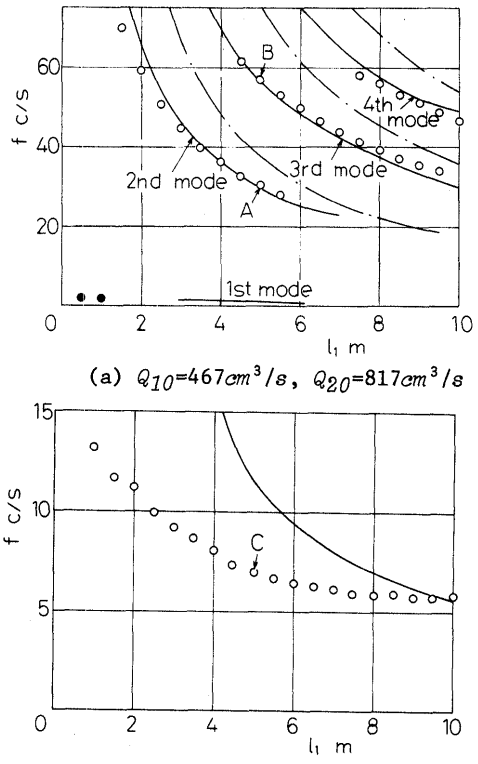

(a) $Q_{10}=467cm^3/s$, $Q_{20}=817cm^3/s$

(b) $Q_{10}=817cm^3/s$, $Q_{20}=467cm^3/s$

(d_f=10mm, l_2=0.5m, V_1=3.9l, V_2=2l)

Fig.8 Frequencies of the oscillation for the double-capacity-oscillator

proportional to velocity in each section was taken into consideration. It is seen from Fig.8(a) that a number of sustained oscillations were observed when $Q_{10}<Q_{20}$. Frequencies of these oscillations coincided with the natural frequencies of the 2nd, 3rd, and 4th modes of the conduit-capacity system of the oscillator. Hereafter, the sustained oscillation is called the 1st, or the 2nd, or ··· mode in order of frequency as shown in Fig.8(a). The oscillations indicated by the marks ● corresponding to the 1st mode of the numerical ones are the relaxation oscillations different from the 1st mode of the above mentioned nutural oscillation. The analytical result (II) in section 3.1 states that a small deviation from the equilibrium state of the system can induce a diverging oscillation with an infinite number of modes when $Q_{10}<Q_{20}$ as far as friction forces in the conduits are ignored. Figure 8(a) shows that in the actual case with friction forces these small divergent oscillations grow into a finite number of periodic oscillations by the effect of the nonlinearity of the system. On the other hand, the system can oscillate at only one frequency at most when $Q_{10}>Q_{20}$ [see (III) in section 3.1]. Only one sustained oscillation was observed for a certain operational condition as in Fig.8(b) in this case, and the imaginary part of the unstable roots of Eq.(11.a) was equal to zero. This means that the solution diverging in a non-oscillatory fashion from the equilibrium state grows up to be a periodic oscillation by the effect of the nonlinearity of the system. It is seen from the figure that the observed values are in good agreement with the theoretically predicted ones when $Q_{10}<Q_{20}$ [see Fig. 8(a)]. However, there is some difference between the observed and the theoretical values when $Q_{10}>Q_{20}$ [see Fig.8(b)]. This difference may be understood as follows: Figures 9(a) and 9(b) are wave forms of the numerical solutions for the model when Q_{10}= 467 and Q_{20}=817 cm^3/s and for the model Q_{10}= 817 and Q_{20}=467 cm^3/s, respectively. The flow rates Q_1 and Q_2 in the both inlet passages of the valve are of the same order of magnitude and are in a phase opposite to each other when $Q_{10}<Q_{20}$. This means that the fluid in the both inlet passages moves as a solid body. Hence, the frequencies of higher modes in Fig.8(a) may coincide with the natural frequencies of the conduit-capacity system mentioned above. On the other hand, the variation of Q_1 is considerably larger than Q_2, and Q_1 and Q_2 oscillate in the same phase during half the period and in an opposite phase during the other half of the period when $Q_{10}>Q_{20}$. It may be concluded that the effect of flow in the vortex chamber on oscillations is more complicated when $Q_{10}>Q_{20}$ than when $Q_{10}<Q_{20}$. Therefore, the difference between the measured and the theoretical frequencies in Fig.8(b) may be caused by the assumption that the characteristics of the vortex valve in operation are the same as the steady state ones. The characteristics in operation deviate increasingly from the steady state ones as frequency of oscillations increases[2]. Figure 10 shows the amplitude of pressure fluctuation $\hat{p}_i$ along the conduit, where the amplitude $|\hat{p}_i|$ is normalized by the value p_1 at the valve side end of the conduit 1, and the phase angle θ is shown with reference to the value at the valve side end of the conduit 1. The positions $z/l=0$ and $z/l=1$ ($l=l_1+l_2$) mean the positions of the capacity side end of the

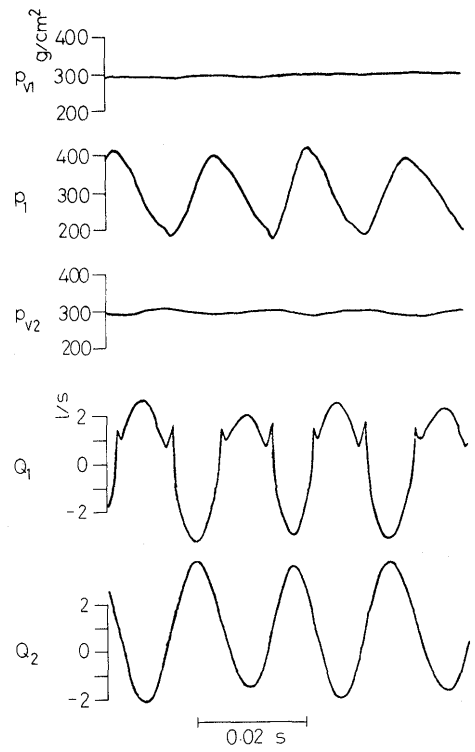

(a) $Q_{10}=467cm^3/s$, $Q_{20}=817cm^3/s$

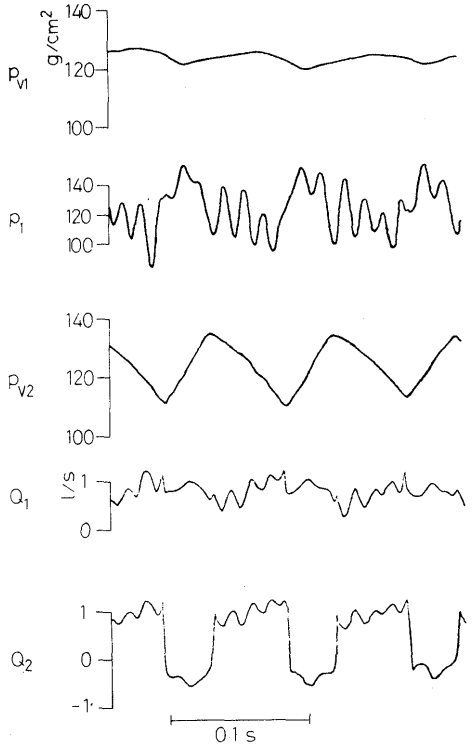

(b) $Q_{10}=817cm^3/s$, $Q_{20}=467cm^3/s$

(d_f=10mm, l_1=5m, l_2=0.5m, V_1=3.9l, V_2=2l)

Fig.9 Wave forms for the double-capacity-oscillator obtained with a digital computer

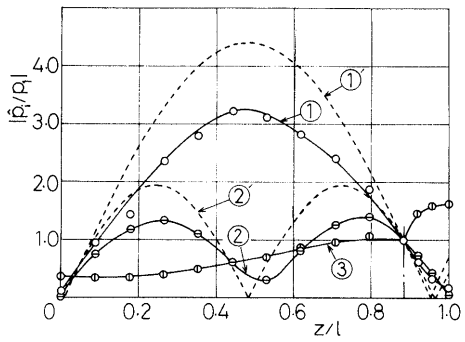

(a) Amplitude distribution

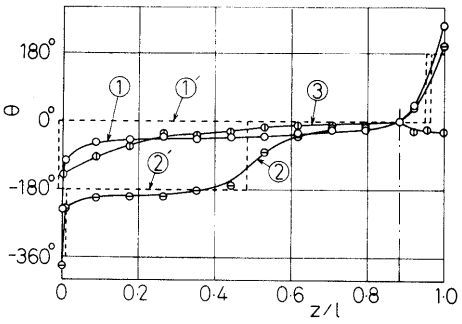

(b) Phase lag

(d_f=10mm, V_1=3.9 , V_2=2l, l_1=5m, l_2=0.5l)

Curve: ① Q_{10}=467cm^3/s, Q_{20}=817cm^3/s, the second mode
② Q_{10}=467cm^3/s, Q_{20}=817cm^3/s, the third mode
③ Q_{10}=817cm^3/s, Q_{20}=467cm^3/s

Fig.10 Pressure fluctuation distribution along the conduit

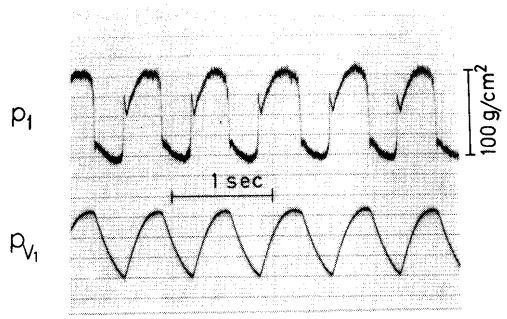

(a) l_1=2 m

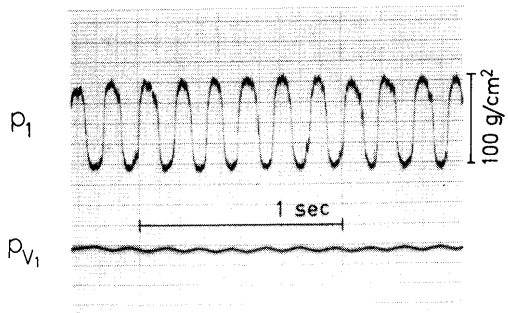

(b) l_1=12 m

(d_f=6mm, V_1=2l, Q_{10}=400cm^3/s, Q_{20}=666cm^3/s)

Fig.11 Examples of the waveforms for the single-capacity-oscillator obtained from the experiments

conduits 1 and 2, respectively. The solid lines ①, ② and ③ correspond to the points A, B and C in Fig.8. The values $|\hat{p}_i|$ and θ were obtained from the fundamental frequency component of the measured wave form. The broken lines ①′, ②′ correspond to the 2nd and 3rd modes of the natural vibration of the conduit-capacity system of the oscillator. The experimental results of the double-capacity-oscillator have been described in the above. The results of the single-capacity-oscillator are given in the following paragraph.

Examples of the measured wave forms are shown in Fig.11. Measured frequency f for various values of the capacity volume V_1 is plotted against the conduit length l_1 in Fig. 12. The solid lines indicate numerical frequencies which were obtained from the fundamental equations, where the lumped parameter system was also used instead of Eqs. (4.a)(4.b). The broken lines show the calculated frequencies corresponding to the typical relaxation oscillation in an extreme case where the mass effect of the fluid in the conduit is ignored. All the observed oscillations in Fig.12(a) over the range of lengths l_1 shown in the figure were the relaxation oscillations and the measured

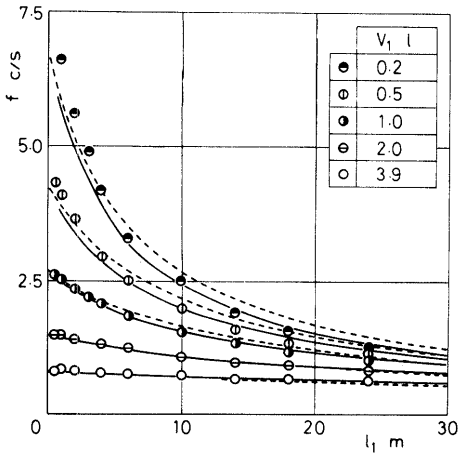

(a) d_f=10 mm

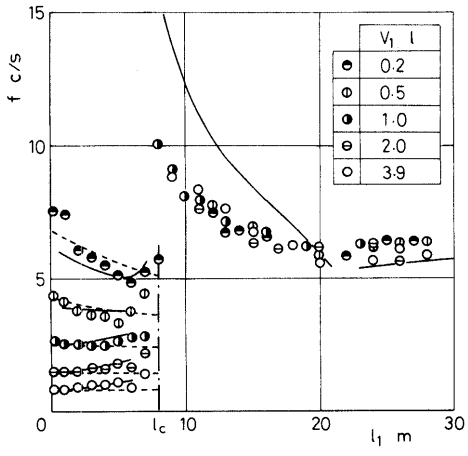

(b) d_f=6 mm

(Q_{10}=400cm^3/s, Q_{20} =666cm^3/s)

Fig.12 Frequencies of the oscillation for the single-capacity-oscillator

frequencies are in good agreement with the analytically predicted ones. It is seen from Fig.12(b) that a sudden change of modes occurs when l_1=7 m. This phenomenon can be understood as follows: When the compressibility and the mass of the fluid in the conduit are ignored, the stability condition becomes $D=E_1+\eta\rho>0$ from the previous paper[2], where η is the coefficient of the conduit friction resistance. There exists a critical conduit length l_c at which the system becomes stable, i.e. D=0, even if $E_1<0$. The relaxation oscillations occur if the length l_1 is smaller than l_c, and no oscillation occurs if $l_1>l_c$. Howevere, when $E_1<0$, higher modes of oscillation occur in a real system having the compressibility and the mass of the fluid even if $l_1>l_c$. The calculated value of l_c shown in Fig.12(b) with a dot-dash line agrees with the measured and numerical results. The higher modes obtained from the numerical calculations were almost independent of the values of V_1.

5. Conclusions

The oscillatory phenomena occurring in a confined type vortex oscillator have been examined theoretically and experimentally. The results obtained from the experiments are in good agreement with the results predicted theoretically.

The authors wish to express their gratitude to Prof. Tadaya Ito, Nagoya Univ., for valuable discussion.

References

(1) Surpkaya, T., et al., *Trans. ASME*, Ser.D, 91-4(1969-12), p.750.
(2) Ito, T., Takagi, S., et al., *Bull. JSME*, 20-147(1977-9), p.1153.
(3) Pinney, E., *Ordinary Difference-Differential Equations*, (1958), p.61, Univ. California Press.
(4) Zalmonzon, L. A., *Theory of Fluidic Elements*, (1969), p.222, Moscow.